1-1-2013

Spinel LiNixMn2-xO4 as cathode material for aqueous rechargeable lithium batteries

F X. Wang
Fudan University

S Y. Xiao
Fudan University

Y Shi
University of Wollongong, ys099@uowmail.edu.au

L L. Liu
Fudan University

Y S. Zhu
Fudan University

See next page for additional authors

Spinel LiNixMn2-xO4 as cathode material for aqueous rechargeable lithium batteries

Abstract

Ni-doped spinel LiNixMn2-xO4 (x = 0, 0.05, 0.10) samples were prepared by a sol-gel method. Structure and morphology of the samples were characterized by X-ray diffraction, scanning electron microscopy, Brunnauer-Emmet-Teller method and inductively coupled plasma atomic absorption spectrometry. The electrochemical behavior as a cathode material (positive mass) for aqueous rechargeable lithium batteries (ARLBs) was investigated by cyclic voltammetry, electrochemical impedance spectroscopy, capacity measurements and cycling tests. The results show that the LiNi 0.1Mn1.9O4 electrode presents the best rate and cycling performance but low reversible capacity. In contrast, the LiNi 0.05Mn1.95O4 electrode shows a higher reversible capacity and relatively good cycling behavior. At a current density of 150 mA g-1, LiNi0.05Mn1.95O4 delivers a reversible capacity of 102 mA h g-1. At the relative high current densities of 1500 and 3000 mA g-1, the LiNi 0.05Mn1.95O4 electrode still delivers reversible capacities of 95.0 and 88.7 mA h g-1, respectively. The Ni-doped samples show excellent cycling life in 0.5 mol L-1 Li 2SO4 aqueous solution. The capacity retention ratios for LiNi0.05Mn1.95O4 and LiNi0.10Mn 1.90O4 after 800 cycles at a current density of 1500 mA g-1 are 79.4% and 91.1%, respectively, much higher than that for the undoped LiMn2O4 at only 37.8%. 2013 Elsevier Ltd. 2013 Elsevier Ltd. All rights reserved.

Keywords

xo4, linixmn2, lithium, rechargeable, batteries, aqueous, spinel, material, cathode

Disciplines

Engineering | Physical Sciences and Mathematics

Publication Details

Wang, F. X., Xiao, S. Y., Shi, Y., Liu, L. L., Zhu, Y. S., Wu, Y. P., Wang, J. Z. & Holze, R. (2013). Spinel LiNixMn2-xO4 as cathode material for aqueous rechargeable lithium batteries. Electrochimica Acta, 93 (March), 301-306.

Authors

F X. Wang, S Y. Xiao, Y Shi, L L. Liu, Y S. Zhu, Y P. Wu, J. Z. Wang, and R Holze

Spinel $LiNi_xMn_{2-x}O_4$ as cathode material for aqueous rechargeable lithium batteries

F.X. Wang [a], S.Y. Xiao [a], Y. Shi [a,b], L.L. Liu [a], Y.S. Zhu [a], Y.P. Wu [1,a],*, J.Z. Wang [b,*] R. Holze [1,c,*]

[a]New Energy and Materials Laboratory (NEML), Department of Chemistry & Shanghai Key Laboratory of Molecular Catalysis and Innovative Materials, Fudan University Shanghai 200433, China

[b]Institute for Superconducting and Electronic Materials, University of Wollongong, Australia

[c]Technische Universität Chemnitz, Institut für Chemie, AG Elektrochemie, D-09107 Chemnitz, Germany

Abstract

Ni-doped spinel $LiNi_xMn_{2-x}O_4$ (x = 0, 0.05, 0.10) samples were prepared by a sol-gel method. Structure and morphology of the samples were characterized by X-ray diffraction, scanning electron microscopy, Brunnauer-Emmet-Teller method and inductively coupled plasma atomic absorption spectrometry. The electrochemical behavior as a cathode material (positive mass) for aqueous rechargeable lithium batteries (ARLBs) was investigated by cyclic voltammetry, electrochemical impedance spectroscopy, capacity measurements and cycling tests. The results show that the $LiNi_{0.1}Mn_{1.9}O_4$ electrode presents the best rate and cycling performance but low reversible capacity. In contrast, the $LiNi_{0.05}Mn_{1.95}O_4$ electrode shows a higher reversible capacity and relatively good cycling behavior. At a current density of 150 mA g^{-1}, $LiNi_{0.05}Mn_{1.95}O_4$ delivers a reversible capacity of 102 mAh g^{-1}. At the relative high current densities of 1500 and

[1] ISE Member
[*] Correspondence, wuyp@fudan.edu.cn (Wu), jiazhao@uow.edu.au (Wang), rudolf.holze@chemie.tu-chemnitz.de (Holze).

3000 mA g^{-1}, the $LiNi_{0.05}Mn_{1.95}O_4$ electrode still delivers reversible capacities of 95.0 and 88.7 mAh g^{-1}, respectively. The Ni-doped samples show excellent cycling life in 0.5 mol L^{-1} Li_2SO_4 aqueous solution. The capacity retention ratios for $LiNi_{0.05}Mn_{1.95}O_4$ and $LiNi_{0.10}Mn_{1.90}O_4$ after 800 cycles at a current density of 1500 mA g^{-1} are 79.4 % and 91.1 %, respectively, much higher than that for the undoped $LiMn_2O_4$ at only 37.8 %.

Keywords: Aqueous rechargeable lithium battery; cathode; $LiMn_2O_4$; Ni doping; electrochemical performance

1. Introduction

Lithium ion batteries (LIBs) have become one of the most important energy storage technologies today in particular for mobile and portable applications. They were invented in the early 1990s, and now are widely used as power sources for electronic devices such as laptops, cellular phones, electric power tools etc. [1 - 3]. Spinel-type $LiMn_2O_4$ and its derivatives have been used as cathode material for the lithium ion batteries because of their low cost, abundance in natural sources, and easy preparation [2]. The electrochemistry of $LiMn_2O_4$ in organic electrolytes has been extensively studied over the past two decades [4 - 10]. Although lithium ion batteries are considered to be the most successful electrochemical devices with high energy density, they are still associated with the risk of safety accidents because of the flammability of the organic electrolytes and improper use such as overcharging or short-circuiting. Moreover, the spinel $LiMn_2O_4$ in the organic electrolyte solutions does not present as excellent cycling life as $LiFePO_4$ due the instability of the spinel structure and the dissolution of manganese into the electrolyte solution during cycling [11, 12]. As a result, the urgent environmental and economic problems unceasingly promote the further development of safer, less expensive and greener battery materials and devices.

To solve these problems, an attractive approach is to use an aqueous electrolyte solution for lithium batteries, in which Li^+-ions are reversibly intercalated into and deintercalated from the active masses with a subsequent charge transfer similar to that in the organic lithium ion battery. In the middle of the 1990s, a rechargeable lithium battery with an aqueous electrolyte was developed [13, 14]. Obviously, the cost of aqueous rechargeable lithium batteries (ARLBs) will be low since electrode and electrolyte materials are not expensive and its assembling process is easy. In addition, it is inherently safe by avoiding the use of flammable organic electrolytes. Moreover, the ionic conductivity of aqueous electrolytes is high, about two orders of magnitude

higher than that of organic electrolytes [15], which ensures high rate capability and thus high specific power. Therefore, ARLBs have received wide interest especially in recent years [15 - 26]. However, the traditional micrometer-sized materials do not show good electrochemical performance in an aqueous electrolyte [18]. Recently, nanostructured $LiMn_2O_4$ samples were prepared and their electrochemical properties, especially reversible capacity, rate capability and cycling life as cathode materials for the ARLBs, have been markedly improved [24 - 28]. For example, a porous $LiMn_2O_4$ consisting of nanograins shows still 93 % capacity retention even after 10000 full cycles [24]. It is known that the uniformity of nanostructured $LiMn_2O_4$ is not easy to control. The use of traditional micrometer-sized materials will be of great promise for the practical application of ARLBs. In order to achieve this goal, doping micrometer-sized $LiMn_2O_4$ with several cations (such as Co, Al, Cr and Mg) would be a good way, which has been proved to reduce Jahn-Teller distortion effectively in organic electrolyte [5, 10, 29, 30]. However, few studies about cation-doped $LiMn_2O_4$ (only Cr, Al, Fe [16, 18, 20]) in aqueous electrolyte have been reported up to now. Herein we report for the first time the electrochemical behavior of spinel-type $LiNi_xMn_{2-x}O_4$ (x = 0, 0.05, 0.1) as cathode materials for aqueous rechargeable lithium batteries. We found, that Ni-doping of $LiMn_2O_4$ can greatly improve its rate behavior and capacity retention at large current densities in aqueous electrolyte.

2. Experimental

The synthesis of spinel $LiNi_xMn_{2-x}O_4$ (x = 0, 0.05, 0.10) particles was carried out according to a previously reported method [29, 30] with minor modifications. Briefly, stoichiometric amounts of lithium acetate [$Li(CH_3COO)\cdot 2H_2O$](0.01 mol), manganese acetate [$Mn(CH_3COO)_2\cdot 4H_2O$], and nickel acetate [$Ni(CH_3COO)_2\cdot 4H_2O$] with the atomic ratio Li : Ni : Mn = 1.05 : x : (2-x), where x is 0, 0.05 and 0.10, respectively, were dissolved in distilled water and mixed with an aqueous solution of citric acid. The citric acid was used as a chelating agent and a fuel for combustion (the molar ratio of carboxylic acid groups in citric acid to metal ions was fixed at 1:1). Then ammonia was added slowly to this solution with constant stirring until a pH of about 7 was achieved. The resultant solutions were evaporated at 80 °C until transparent sols were obtained. To remove water, the obtained precursors were dried under vacuum at 120 °C over-night. The resulting gel precursors were burned at 450 °C for 6 h, then 800 °C for 10 h in air. The rate of temperature increase was 3 $^oC\ min^{-1}$. All chemicals were of analytical grade, and the solutions were prepared with distilled water.

The electrodes were prepared by mixing powdered samples, acetylene black and poly-tetrafluoroethylene (PTFE) in a weight ratio of 8:1:1 with the help of ethanol. The mixture was pressed into a film, and then dried at 120 ^oC overnight to act as working electrodes. After dry-ing, the film was cut into disks of about 2 mg (0.36 cm^2 in area and 0.4 mm in thickness). These disks were pressed onto a Ni-grid at a pressure of 20 MPa to act as the working electrodes. Cyclic voltammetry (CV), electrochemical impedance measurements, and the first charge-discharge profiles of the $LiNi_xMn_{2-x}O_4$ (x = 0, 0.05 and 0.10) electrodes were performed in 0.5 mol L^{-1} Li_2SO_4 solution (small amounts of LiOH were added to ensure its pH value is 7) with a three-electrode cell, in which a Ni-grid and a saturated calomel electrode (SCE) were used as counter and reference electrodes, respectively. The CV data were collected between 0 and 1.2 V

(*vs*. SCE) at different scan rates. The $LiNi_xMn_{2-x}O_4$ electrodes were charged and discharged in the potential range of 0.3 - 1.05 V (*vs*. SCE) at various current densities. The electrochemical impedance spectra (EIS) were recorded from 10^5 to 0.1 Hz.

Activated carbon (AC) with a specific surface area of about 2800 $m^2 g^{-1}$ measured by a Brunauer–Emmet–Teller (BET) method was purchased from Ningde Xinseng Chemical Industrial Co., Ltd. and used as received without further treatment. The activated carbon electrodes were prepared in the same way as the $LiNi_xMn_{2-x}O_4$ (x = 0, 0.05, 0.10) electrodes [18]. Since it can absorb and desorb Li^+ ions very quickly, it will not have any adverse effects on the properties of the working electrodes [24]. A two-electrode cell consisting of the above $LiNi_xMn_{2-x}O_4$ (x = 0, 0.05, 0.10) working electrode and the activated carbon counter electrode with a distance of about 1 cm was used to test the cycling behavior of the as-prepared samples in 0.5 mol L^{-1} Li_2SO_4 solution on a cell tester (Land 2001A). The mass ratio of the spinel $LiNi_xMn_{2-x}O_4$ (x = 0, 0.05, 0.10) to the activated carbon was fixed at about 1:3.5. All tests were carried out at room temperature.

The X-ray diffraction (XRD) patterns were collected using a Rigaku D/MAX-IIA X-ray diffractometer with Cu Kα radiation. Data were collected in a step-scan mode in the range of 10 – 90° with intervals of 8° min^{-1}. Scanning electron micrographs (SEM) were obtained on a Philips microscope XL30 operated at 25 kV. The specific area was measured according to the BET method using a Micromeritics Tristar ASAP 3000 BET apparatus with liquid nitrogen at 77 K. Elemental analysis was obtained on a Thermo E. IRIS Duo inductively coupled plasma atomic absorption spectrometer (ICP-AAS).

3. Results and discussion

The XRD patterns of the as-prepared samples $LiNi_xMn_{2-x}O_4$ (x = 0, 0.05, 0.10) are shown in Fig. 1. The diffraction peaks can be indexed to the spinel with a space group *Fd3m*, they are in good agreement with the standard pattern (JCPDS, Card No.35-0782) [31]. Fig. 2 shows the SEM micrographs of the samples. Their particle sizes are in the sub-micrometer range from 200 to 400 nm. There is not much difference in the morphology since the preparation method is the same for all samples and compositions. Table 1 lists the chemical compositions and surface areas of the samples. For the as-prepared samples, the experimental Ni/Mn ratios agree basically with the target stoichiometry. The BET specific surface area of the samples are 2.30, 2.09 and 1.97 $m^2\ g^{-1}$, respectively, for $LiMn_2O_4$, $LiNi_{0.05}Mn_{1.95}O_4$ and $LiNi_{0.10}Mn_{1.9}O_4$. The reason for these differences needs further study.

The CVs of the samples at different scan rates are presented in Fig. 3(a-c). There are two redox couples at low scan rates. The anodic and cathodic peaks correspond to lithium de-intercalation and intercalation. The splitting of the redox peaks into two couples shows, that the electrochemical reaction of the de-intercalation and intercalation of Li^+ ions consists of two processes, which is consistent with the results in both organic and aqueous electrolytes [2, 5, 6, 12, 19, 24, 33, 34]. At the low scan rate, two separate couples of redox peaks can be observed for all electrodes. At the lowest scan rate (1 mV/s), the anodic current peak of the doped sample ($LiNi_{0.10}Mn_{0.90}O_4$) is less well-defined in comparison to those of the undoped phase ($LiMn_2O_4$), which indicates that the substitution of nickel ions may eliminate the small Li-Li repulsion energy difference between the half-filled 8a sites in $Li_{0.5}Mn_2O_4$ and the completely filled sites in $LiMn_2O_4$ [11, 29].

With increasing scan rate, the separation between the two redox pairs becomes smaller. It is noted that the peaks of Ni-doped samples retain the well-defined shape when the scan rate

increases to 8 mV s^{-1} (Fig. 3b and c), which indicates that the Ni doped electrodes can be charged and discharged at larger current densities. In contrast, the peaks of the undoped $LiMn_2O_4$ become less distinguishable at this scan rate (Fig. 3a). When the scan rate continues to increase to 10 mV s^{-1}, the $LiNi_{0.1}Mn_{1.9}O_4$ electrode still retains the well-defined shape, which implies that it will present the best rate behavior.

The Nyquist plots (Fig. 3d) of the $LiNi_xMn_{2-x}O_4$ (x = 0, 0.05 and 0.1) electrodes show a semicircle at mid-high frequency and a linear region at low frequencies. The linear region corresponds to the diffusion process of Li^+-ions in the electrode. The semicircles correspond to a parallel combination of charge-transfer resistance (R_{ct}) and double-layer capacitance [24, 35]. The R_{ct} values can be estimated from the diameter of the semicircle on the real axis. It can be seen that the Ni-doped samples exhibit a smaller R_{ct} than the undoped one, suggesting that the doping of a certain amount of Ni ions could effectively decrease the charge transfer resistance in the spinel. The first charge-discharge profiles of the $LiNi_xMn_{2-x}O_4$ (x = 0, 0.05 and 0.10) electrodes in the aqueous electrolyte at different current densities are shown in Fig. 4. There are two distinct charge and discharge plateaus, which reflect a two-stage Li^+-ion de-intercalation and intercalation behavior and consistent with both the obtained CV curves and other reports [5, 6]. For the $LiNi_{0.1}Mn_{1.9}O_4$ electrode the plateaus became less distinct, suggesting that the local distortion of the host structure resulting from the substitution of nickel ions may eliminate the small Li-Li repulsion energy difference between the half-filled 8a sites in $Li_{0.5}Mn_2O_4$ and the completely filled sites in $LiMn_2O_4$ [11, 29, 36].

At a charge/discharge current density of 150 mA g^{-1} (Fig. 4a) the $LiMn_2O_4$ electrode exhibits initial discharge capacities of 103 mAh g^{-1}, higher than $LiNi_{0.05}Mn_{1.95}O_4$ electrode (102 mAh g^{-1}) and $LiNi_{0.1}Mn_{1.9}O_4$ electrode (83.0 mAh g^{-1}). Substitution was found to decrease the capacity by reducing the quantity of oxidisable Mn^{3+}. This is similar to the doping effects of $LiNi_xMn_{2-x}O_4$

in the organic electrolytes [5, 10]. The initial capacities of the electrodes decrease with the increasing current density. At the current density of 300 mA g^{-1} (Fig. 4b), the $LiMn_2O_4$, $LiNi_{0.05}Mn_{1.95}O_4$ and $LiNi_{0.10}Mn_{1.90}O_4$ electrodes deliver discharge capacities of 97.2, 101 and 74.1 mAh g^{-1}, respectively. Even at the relative high current density of 1500 and 3000 mA g^{-1} (Fig. 4c and d), the $LiNi_{0.05}Mn_{1.95}O_4$ electrodes still deliver discharge capacities of 95.0 and 88.7 mAh g^{-1}, respectively. The capacities for $LiNi_{0.10}Mn_{1.90}O_4$ electrodes are 71.9 and 69.0 mAh g^{-1} at 1500 and 3000 mA g^{-1}, respectively. However, the undoped spinel $LiMn_2O_4$ electrodes deliver only 83.9 and 67.2 mAh g^{-1} at the same current densities. For the $LiNi_{0.05}Mn_{1.95}O_4$ electrode, these improved properties are further confirmed in the rate capabilities test at the current density ranging from 300 to 5000 mA g^{-1} (Fig. 5). Fig. 5 suggests that the $LiNi_{0.1}Mn_{1.9}O_4$ electrode presents the best rate behavior, but its reversible capacity is lower. The $LiNi_{0.05}Mn_{1.95}O_4$ electrode shows better rate capabilities and could deliver 99.8 mAh g^{-1} at the charge/discharge current density of 1000 mA g^{-1}. In contrast, the undoped $LiMn_2O_4$ and $LiNi_{0.1}Mn_{1.9}O_4$ exhibit discharge capacities of 83.8 and 73.8 mAh g^{-1}, respectively. Moreover, after 50 cycles, as the charge and discharge current densities are reduced from 5000 to 300 mAh g^{-1}, the discharge capacity of the doped $LiNi_{0.05}Mn_{1.95}O_4$ and $LiNi_{0.1}Mn_{1.9}O_4$ electrodes recovered nearly without capacity loss, but the undoped spinel shows more than 9 % capacity fading.

The cycling performance of $LiNi_xMn_{2-x}O_4$ (x = 0, 0.05, 0.10) electrodes measured by using activated carbon (AC) as the anode in a potential range of 0 - 1.8 V is shown in Fig. 6. After 300 cycles at the current density of 300 mA g^{-1}, the capacity of the undoped cathode material decreases to 78.9 mAh g^{-1}, about 76.6 % capacity retention. In contrast, the $LiNi_{0.05}Mn_{1.95}O_4$ electrode fades from 102 to 89.7 mAh g^{-1}, about 87.9 % capacity retention, which is superior to that reported with aqueous electrolyte [15, 16, 18, 23]. For the $LiNi_{0.1}Mn_{1.9}O_4$ electrode, though its

reversible capacity is the smallest, it only fades from 76.9 to 73.1 mAh g^{-1}, about 95.1% capacity retention after 300 cycles. After 800 cycles at a current density of 1500 mAg^{-1}, the discharge capacity of the undoped $LiMn_2O_4$ decreases rapidly to 31.6 mAh g^{-1}. Similar to the cycling at the low current density, the doped $LiNi_xMn_{2-x}O_4$ electrodes also present better cycling performance. The $LiNi_{0.05}Mn_{1.95}O_4$ and $LiNi_{0.10}Mn_{1.90}O_4$ can still retain 74.9 (79.4 %) and 71.9 mAh g^{-1} (91.1 %). It is clear that Ni-doping can effectively improve the cycling performance of the spinel $LiMn_2O_4$. One reason for this improvement is that the doped Ni-ions enhance the stability of the octahedral sites in the spinel structure due to the stronger Ni-O bond (bond energy: 1029 kJ mol^{-1}) [37]. In the case of α-MnO_2, the bond energy of Mn-O is 946 kJ mol^{-1}. Moreover, substitution of manganese by Ni ions decreases the concentration of Mn^{3+} and reduces the Jahn-Teller distortion [29, 30]. The smaller capacity of the $LiNi_{0.10}Mn_{1.90}O_4$ can also be partly attributed to the lattice contraction [37] beside less Mn^{3+} ions.

4. Conclusions

In summary, the Ni-doped spinel-type $LiNi_xMn_{2-x}O_4$ (x = 0, 0.05, 0.10) cathode materials were prepared by a sol-gel method. The $LiNi_{0.05}Mn_{1.95}O_4$ electrode shows a higher reversible capacity and relatively good rate behavior. At a current density of 150 mA g^{-1}, the $LiNi_{0.05}Mn_{1.95}O_4$ electrodes deliver a discharge capacity of 102 mAh g^{-1}. Even at the relative high current density of 1500 and 3000 mA g^{-1}, the $LiNi_{0.05}Mn_{1.95}O_4$ electrode still deliver initial discharge capacities of 95.0 and 88.7 mAh g^{-1}, respectively. Ni ion substitution can reduce capacity fading of spinel $LiMn_2O_4$ during cycling in 0.5 mol L^{-1} Li_2SO_4 aqueous solution. After 800 cycles, the discharge capacity of the $LiNi_{0.05}Mn_{1.95}O_4$ electrode fades from 94.3 to 74.9 mAh g^{-1} with the loss of 20.6 % of its initial capacity at a current density of 1500 mA g^{-1}. Although the reversible capacity of

the $LiNi_{0.1}Mn_{1.9}O_4$ electrode is the smallest it fades only from 71.0 to 64.7 mAh g^{-1}, about 91.1 % capacity retention.

Acknowledgments

The authors acknowledge financial support from MOST Programs (2010DFA61770), NSFC (21073046) and an Australian Research Council (ARC) Discovery Project (DP100103909).

References:

[1] P. Simon, Y. Gogotsi, *Nat. Mater.* 7 (2008) 845.

[2] Y.P.Wu, X.B. Dai, J.Q. Ma, Y.J. Cheng, *Lithium Ion Batteries: Practice and Applications, Chemical Industry Press*, Beijing, 2004.

[3] J. M. Tarascon, M. Armand, *Nature* 414 (2001) 359.

[4] W. Tang, X.J. Wang, Y.Y. Hou, L.L. Li, H. Sun, Y.S. Zhu, Y. Bai, Y.P. Wu, K. Zhu, T. van Ree, *J. Power Sources* 198 (2012) 308.

[5] T. Kakuda, K. Uematsu, K. Toda , M. Sato, *J. Power Sources* 167 (2007) 499.

[6] K.S. Lee, S.T. Myung, K. Amine, H. Yashiro, Y.K. Sun, *J. Mater. Chem.* 19 (2009) 1995.

[7] F. Jiao, J.L. Bao, A.H. Hill, P.G. Bruce, *Angew. Chem. Int. Ed.* 47 (2008) 9711.

[8] D.K. Kim, P. Muralidharan, H.W. Lee, R. Ruffo, Y. Yang, C.K. Chan, H.L. Peng, R.A. Huggins, Y. Cui, *Nano Lett.* 8 (2008) 3948.

[9] K.M. Shaju, Peter G. Bruce, *Chem. Mater.* 20 (2008) 5557.

[10] A. Sakunthala, M. Reddy, S. Selvasekarapandian, B. Chowdari, P. Selvin, *Electrochim Acta* 55 (2010) 4441.

[11] Y.Y. Xia, Y.H. Zhou, M. Yoshio, *J. Electrochem.Soc.* 144 (1997) 2593.

[12] M.M. Thackeray, Y.S. Horn, A.J. Kahaian, K.D. Kepler, J.T. Vaughey, S.A. Hackney, *Electrochem. Solid-State Lett.* 1 (1998) 7.

[13] W. Li, W.R. McKinnon, J.R. Dahn, *J. Electrochem. Soc*. 141 (1994) 2310.

[14] W. Li, J.R. Dahn, D.S. Wainwright, *Science* 264 (1994) 1115.

[15] R. Ruffo, F.L. Mantia, C. Wessells, R.A. Huggins, Y. Cui, Solid State Ionics 192 (2011) 289.

[16] M.S. Zhao, X.P. Song, F. Wang, W.M. Dai, X.G. Lu, *Electrochim. Acta* 56 (2011) 5673.

[17] F. Wang, Y. Liu, C.Y Liu, *Electrochim. Acta* 55 (2010) 2662.

[18] A. Yuan, L. Tian, W. Xu, Y. Wang, *J. Power Sources* 195 (2010) 5032.

[19] R. Ruffo, C. Wessells, R.A. Huggins, Y. Cui, *Electrochem. Commun.* 11 (2009) 247.

[20] W. Xu, A. Yuan, Y. Wang, *J. Solid State Electrochem* 16 (2012) 429.

[21] J.Y. Luo, W.J. Cui, P. He, Y.Y. Xia, *Nat. Chem.* 2 (2010) 760.

[22] J. Y. Luo, Y.Y. Xia, *J. Power Sources* 186 (2009) 224.

[23] P. He, J.Y. Luo, J.X. He, Y.Y. Xia, *J. Electrochem. Soc.* 156 (2009) A209.

[24] Q.T. Qu, L.J.Fu, X.Y. Zhan, D. Samuelis, J. Maier, L.Li, S. Tian, Z.H. Li, Y.P. Wu, *Energy. Environ. Sci.* 4 (2011) 3985.

[25] W. Tang, S. Tian, L.L. Liu, L.Li, H.P. Zhang, Y.B. Yue, Y. Bai, Y.P. Wu, K. Zhu, *Electrochem.Commun.* 13 (2011) 205.

[26] W. Tang, L.L. Liu, S. Tian, L. Li, L.L. Li, Y.B. Yue, Y. Bai, Y.P. Wu, K. Zhu, R. Holze, *Electrochem. Commun.* 13 (2011) 1159.

[27] W. Tang, L.L. Liu, Y.S. Zhu, H. Sun, Y.P. Wu, K. Zhu, *Energy Environ. Sci*. 5 (2012) 6909.

[28] W. Tang, X.W. Gao, Y.S. Zhu, Y.B. Yue, Y. Shi, Y.P. Wu, K. Zhu, *J. Mater. Chem*. 22 (2012), DOI:10.1039/C2JM34563C

[29] Y.K. Sun, S.H. Jin, *J. Mater. Chem.* 8 (1998) 2399.

[30] Y.K. Sun, Y.S. Jeon, *J. Mater. Chem.* 9 (1999) 3147.

[31] C. Bellitto, E.M. Bauer, G. Righini, M.A. Green, W.R. Branford, A. Antonini, M. Pasquali, *J. Phys. Chem. Solids* 65 (2004) 29.

[32] S.S. Zhang, K. Xu, T.R. Jow, *Electrochim. Acta* 49 (2004) 1057.

[33] S.J. Bao, Y.Y. Liang, W.J. Zhou, B.L. He, H.L. Li, *J. Power Sources* 154 (2006) 239

[34] N. Santander, S.R. Das, S.B. Majumder, R.S. Katiyar, *Surf. Coat. Technol.* 60 (2004) 177.

[35] S. Devaraj, N. Munichandraiah, *J.Electrochem. Soc.* 154 (2007) A80.

[36] Y.M. Choi, S.I. Pyun, *Solid State Ionics* 99 (1997) 173.

[37] Y.P. Wu, E. Rahm, R. Holze, *Electrochim. Acta* 47 (2002) 3491.

Captions of Figures and Tables

Fig. 1 XRD patterns of $LiNi_xMn_{2-x}O_4$ (x = 0, 0.05, 0.10) samples.

Fig. 2 SEM micrographs of $LiNi_xMn_{2-x}O_4$ samples: (a) x = 0, (b) x = 0.05, (c) x = 0.1.

Fig. 3 The cyclic voltammograms of the $LiNi_xMn_{2-x}O_4$ samples for (a) x = 0, (b) x = 0.05 and (c) x = 0.1 at different scan rates, and (d) the Nyquist plots of the $LiNi_xMn_{2-x}O_4$ (x = 0, 0.05 and 0.1) electrodes.

Fig. 4 The first charge/discharge profiles of the $LiNi_xMn_{2-x}O_4$ (x = 0, 0.05 and 0.1) samples at charge and discharge current densities of (a) 150, (b) 300, (c) 1500 and (d) 3000 mA g^{-1}.

Fig. 5 Rate capabilities of the $LiNi_xMn_{2-x}O_4$ (x = 0, 0.05 and 0.1) samples at charge–discharge current densities ranging from 300 to 5000 mA g^{-1}.

Fig. 6 Cycling performance of the $LiNi_xMn_{2-x}O_4$ (x = 0, 0.05 and 0.1) samples at a charge and discharge current density of (a) 300 and (b) 1500 mA g^{-1}.

Tab. 1 Chemical composition and BET surface area of the prepared samples.

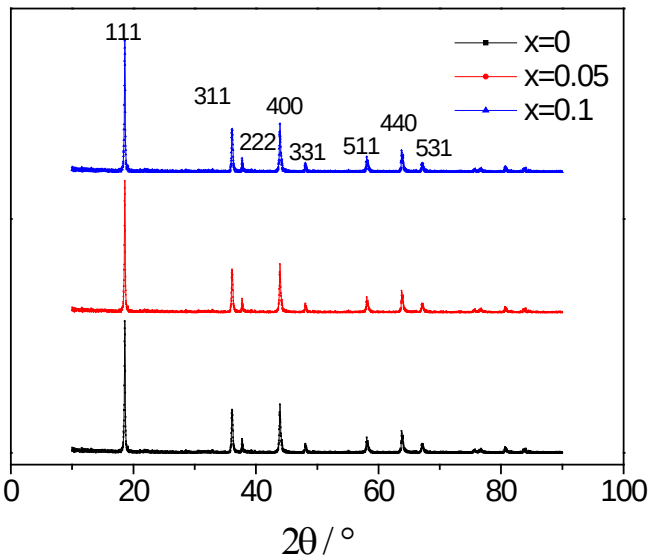

Fig. 1

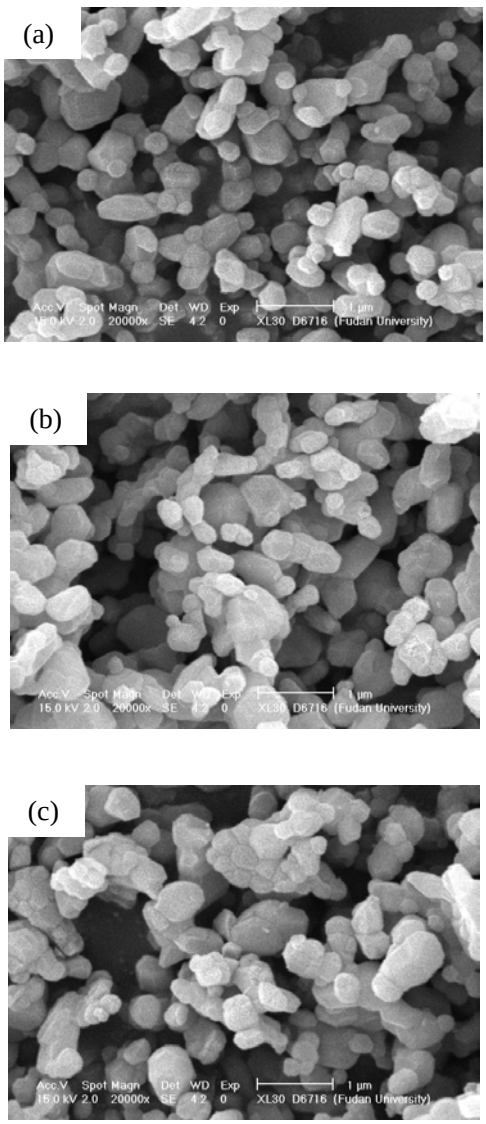
(a)
Acc.V Spot Magn Det WD Exp 1 µm
15.0 kV 2.0 20000x SE 4.2 0 XL30 D6716 (Fudan University)
(b)
Acc.V Spot Magn Det WD Exp 1 µm
15.0 kV 2.0 20000x SE 4.2 0 XL30 D6716 (Fudan University)
(c)
Acc.V Spot Magn Det WD Exp 1 µm
15.0 kV 2.0 20000x SE 4.2 0 XL30 D6716 (Fudan University)

Fig. 2

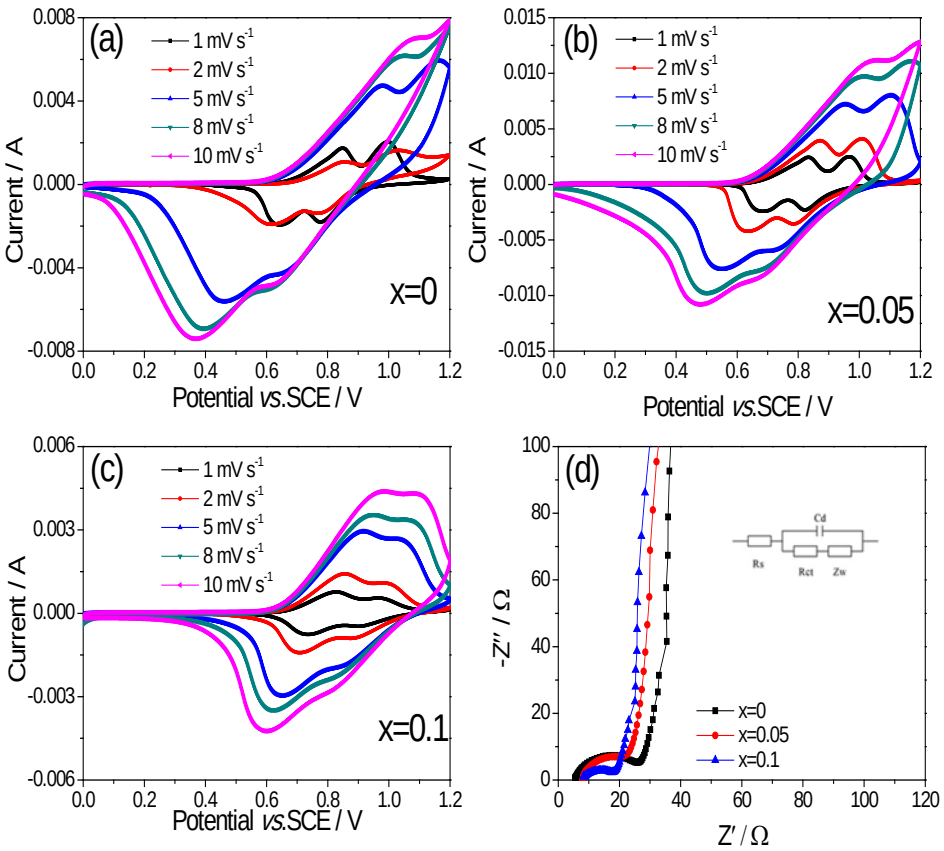
(a)
1 mV s-1
2 mV s-1
5 mV s-1
8 mV s-1
10 mV s-1
x=0
Current / A
Potential vs.SCE / V
(b)
x=0.05
(c)
x=0.1
(d)
Cd
Rs
Rct
Zw
x=0
x=0.05
x=0.1
-Z'' / Ω
Z' / Ω

Fig. 3

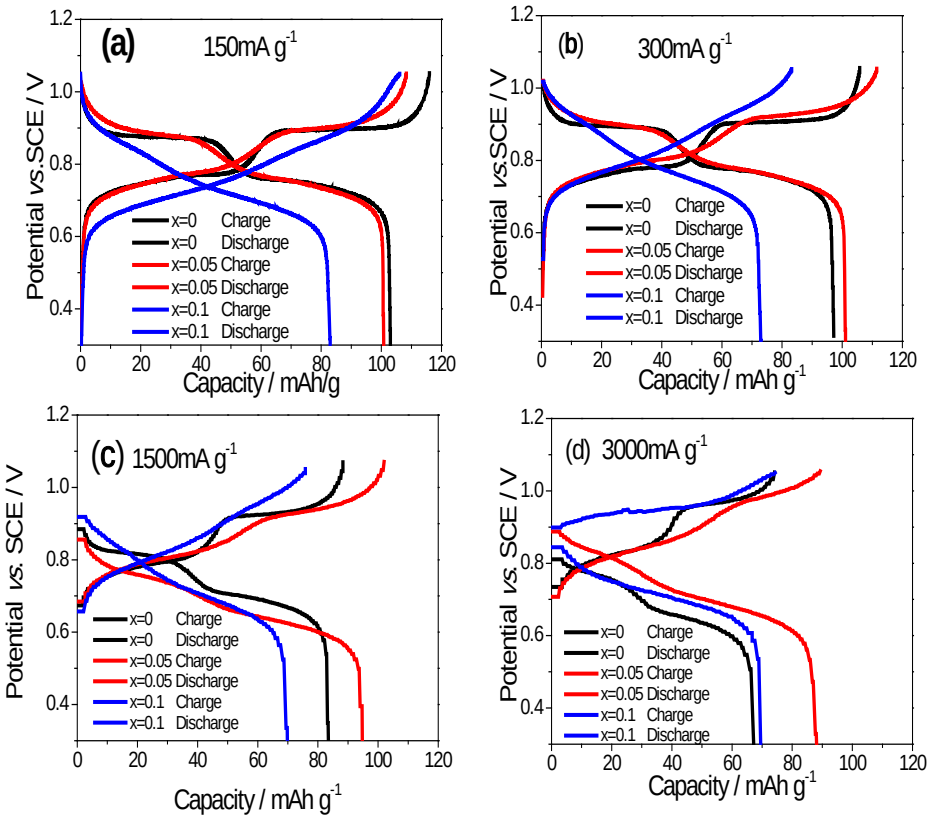
(a) 150mA g-1
Potential vs.SCE / V
Capacity / mAh/g
x=0 Charge
x=0 Discharge
x=0.05 Charge
x=0.05 Discharge
x=0.1 Charge
x=0.1 Discharge
(b) 300mA g-1
Potential vs.SCE / V
Capacity / mAh g-1
(c) 1500mA g-1
Potential vs. SCE / V
Capacity / mAh g-1
(d) 3000mA g-1
Potential vs. SCE / V
Capacity / mAh g-1

Fig. 4

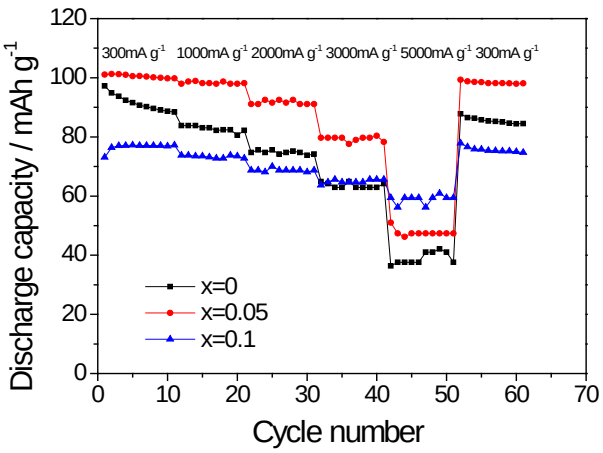
300mA g-1
1000mA g-1
2000mA g-1
3000mA g-1
5000mA g-1
300mA g-1
x=0
x=0.05
x=0.1
Discharge capacity / mAh g-1
Cycle number
0
20
40
60
80
100
120
0
10
20
30
40
50
60
70

Fig. 5

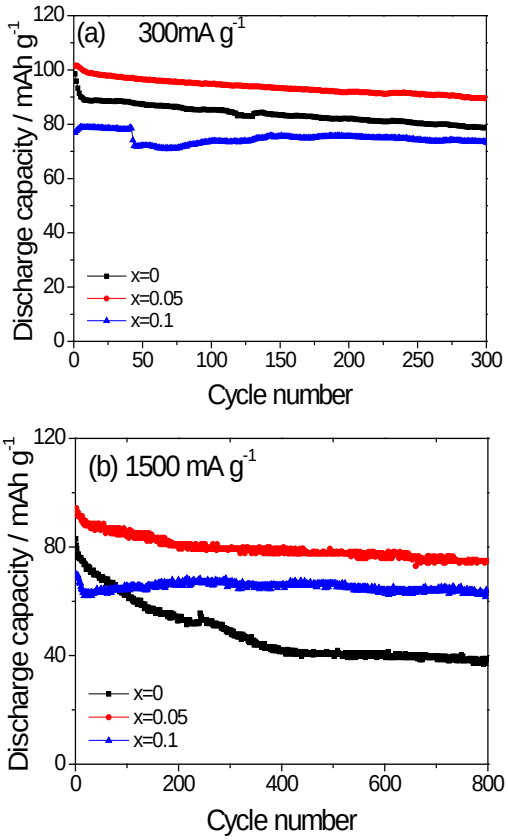
(a) 300mA g-1
Discharge capacity / mAh g-1
Cycle number
x=0
x=0.05
x=0.1
(b) 1500 mA g-1
Discharge capacity / mAh g-1
Cycle number
x=0
x=0.05
x=0.1

Fig. 6

Tab. 1.

Samples: $LiNi_xMn_{2-x}O_4$	x = 0.00	x = 0.05	x = 0.10
Mass fraction of Mn	60.14 %	59.09 %	57.15 %
Mass fraction of Ni	0 %	1.72 %	3.37 %
Molar ratio of Mn:Ni from ICP-AAS	2.00 : 0	1.95 : 0.053	1.90 : 0.105
Theoretical molar ratio of Mn:Ni	2.00 : 0	1.95 : 0.05	1.90 : 0.10
Surface area / $m^2\ g^{-1}$	2.30	2.09	1.97